



## Selective removal of 2,4-dichlorophenol and 2,4,6-trichlorophenol in aqueous solutions by polyaniline-modified magnetic nanoparticles using high-performance liquid chromatography–UV detection

Jasmin Shah<sup>a</sup>, Muhammad Rasul Jan<sup>a</sup>, Behisht Ara<sup>a,\*</sup>, Mian Muhammad<sup>b</sup>, Durr-e-Nayab<sup>a</sup>, Sobi Bibi<sup>a</sup>

<sup>a</sup>Institute of Chemical Sciences, University of Peshawar, Khyber Pakhtunkhwa, Pakistan, emails: bahishtara@gmail.com (B. Ara), jasminshah2001@yahoo.com (J. Shah), rasuljan@yahoo.com (M.R. Jan), durrenayab.ana@gmail.com (Durr-e-Nayab), sobikhan1994@gmail.com (S. Bibi)

<sup>b</sup>Department of Chemistry, University of Malakand, Khyber Pakhtunkhwa, Pakistan, email: mianchem@uom.edu.pk

Received 26 February 2018; Accepted 12 July 2018

### ABSTRACT

The aim of this work was to develop simple, efficient, and environmental friendly adsorbent, polyaniline (PANI)-modified magnetic nanoparticles ( $\text{Fe}_3\text{O}_4$ @PANI) for the removal of 2,4-dichlorophenol and 2,4,6-trichlorophenol from wastewater. Magnetic nanoparticles were synthesized by co-precipitation method and coated with PANI through oxidative polymerization of aniline monomers. The morphology, elemental composition, and crystallinity of ( $\text{Fe}_3\text{O}_4$ @PANI) were determined using scanning electron microscopy, energy dispersion X-ray, X-ray diffraction spectroscopy, and Fourier-transform infrared spectroscopy for functional group analysis, respectively. The parameters effecting the adsorption efficiency such as pH, temperature, contact time, adsorbent dosage, and initial concentration of 2,4-dichlorophenol and 2,4,6-trichlorophenol were studied. The experimental adsorption results were evaluated by different isotherms, and the Freundlich isotherm model was found to best fit the data. Three kinetics models were applied to the data and the pseudo-second-order kinetic model was found leading the kinetics of adsorption process. Thermodynamics evaluation of the adsorption parameters showed that the adsorption is exothermic and spontaneous at low temperature. This research elucidated that ( $\text{Fe}_3\text{O}_4$ @PANI) is efficient, low cost, and environmental friendly adsorbent to remove 2,4-dichlorophenol and 2,4,6-trichlorophenol from wastewater.

*Keywords:* 2,4-Dichlorophenol; 2,4,6-Trichlorophenol; Polyaniline; Magnetic nanoparticles; Oxidative polymerization

### 1. Introduction

The polyaniline (PANI) refers to a very important class of electronic/conducting polymers, commonly referred as a “synthetic metal”. PANI is a polyaromatic amine that can be easily synthesized chemically from Brønsted acidic aqueous solutions [1]. They can be considered as being derived from a polymer, the base form of it (emeraldine base) and protonated emeraldine base (emeraldine hydrochloride) has

the generalized composition given in the scheme (Fig. 1). It consists of alternating reduced, and oxidized, repeat units, which appears to have significant pi delocalization in the polymer backbone. It is an organic polymer from relatively a new class that has shown its functions covering a great range from its use as an insulator to its use as a metal and also depicting the properties of conventional polymer. One of its advantages is the presence of large amounts of amine and imine functional groups [2], porous structure and, therefore, high surface area to volume ratio; and this polymer is

\* Corresponding author.

reported to have interactions with some metal ions and pesticides having strong affinity to nitrogen [3]. Based on these facts, methods have been developed on utilizing PANI as adsorbent to solve environmental problems with excellent selectivity and sorption capacity for the pollutants [4,5]. Likewise PANI and its copolymer nanofibers have shown to have potential for the removal of Co(II) and Cr(VI) ions from aqueous solutions [6–8].  $\text{Fe}_3\text{O}_4@\text{SiO}_2@\text{PANI}$ –graphene oxide composite prepared through a simple noncovalent method has been reported to be used for magnetic solid-phase extraction of trace rare earth elements in tea leaves and environmental water samples [9]. Adsorption interaction of many organic dyes [10–16] is also being demonstrated using emeraldine salt. Some of its other applications include solid-phase extraction of pesticides [17–21]. Among the other most toxic produce of the industries, phenols and phenolic compounds are very important [22]. Because the toxicity and potential harm that it has brought to aquatic life, plants, and human beings, even at low concentrations, phenols and its compounds are considered as main concerned pollutants by the United States Environmental Protection Agency [23]. Chlorophenols are phenolic derivatives with chlorines (between one and five) added to phenol. These compounds are largely provided by chemical industries of pesticides, petroleum refineries, pharmaceuticals, plastics, and wood preservation. They are among the most hazardous anthropogenic compounds, because of their mutagenic, carcinogenic, and teratogenic behavior. 2,4-Dichlorophenol (2,4-DCP) and 2,4,6-trichlorophenol (2,4,6-TCP) are the most commonly used ones. These have been described to create chronic effects on human respiratory and nervous systems. The carbon–chloride bond and its relative position with respect to the hydroxyl group are responsible for their toxicity and persistence in the biological environment. The maximum acceptable concentrations and aesthetic objectives for four chlorophenols in drinking water are given in Table 1 [24]. Due to the high toxicity, carcinogenic properties, structural stabilization, and persistence in the environment, the removal of 2,4-DCP and 2,4,6-TCP from the environment is, therefore, crucial, and the methods reported for its removal includes materials such as heterogeneous catalysts

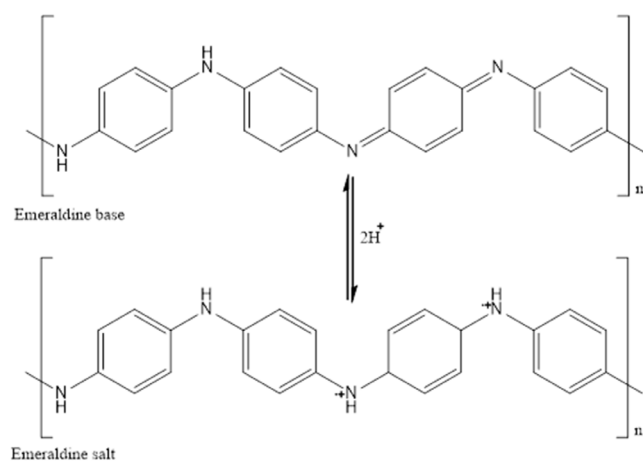


Fig. 1. Generalized chemical composition of PANI as emeraldine base and salt.

like Pd/Fe- $\text{Fe}_3\text{O}_4@\text{MWCNTs}$ , Ni/Fe- $\text{Fe}_3\text{O}_4$ , and graphene oxide/ $\text{Fe}_3\text{O}_4$  [25–28]. However, there are limited methods reported on the removal of this hazardous pollutant from aqueous solutions using  $\text{Fe}_3\text{O}_4@\text{PANI}$ .

The objective of this research work was to prepare iron magnetic nanoparticles by co-precipitation method and the surface coating/stabilization of magnetic nanoparticles with PANI and to explore its use as a solid-phase extraction material for the removal of 2,4-DCP and 2,4,6-TCP from environmental wastewater samples.

## 2. Experimental setup

### 2.1. Reagents and chemicals

All chemicals used were of analytical grade or similar purity. Iron(II) sulfate hepta hydrate ( $M = 278.02$  g/mol, Merck, 64274, Darmstadt, Germany), iron(III) chloride ( $M = 162.21$  g/mol, BDH Laboratory Supplies), and ammonia solution (32%,  $M = 17.03$ , Merck KGaA, 64271, Darmstadt, Germany) were used for the preparation of iron magnetic nanoparticles. Hydrochloric acid ( $M = 36.64\%$ , 35.4%, BDH Laboratory Supplies, Poole, England), potassium persulphate ( $M = 270.32$  g/mol, Merck, 216224, Darmstadt, Germany) as polymerizing agent and aniline ( $M = 93.13$  g/mol, 242284, Sigma-Aldrich, Steinheim, Germany) as monomer were used for the PANI coating of the  $\text{Fe}_3\text{O}_4$  magnetic nanoparticles. Methanol and acetonitrile (494291 and 270717, Sigma-Aldrich, Steinheim, Germany) were used for high-performance liquid chromatography (HPLC) purpose.

### 2.2. Instruments used

JDX-3532 JEOL (Tokyo, Japan) diffractometer with monochromatic Cu-K $\alpha$  radiation ( $\lambda = 1.5418$  Å) at 40 KV and 30 mA in the  $2\theta$  range of  $5^\circ$ – $80^\circ$  with  $1.03^\circ/\text{min}$  was used to obtain X-ray diffraction (XRD) designs of the adsorbents. For elemental analysis, energy dispersive X-ray (EDX) analysis mapping of the adsorbents were obtained using EDX-INCA 200, Oxford Instruments, UK. The surface morphology and physical nature of the adsorbent were examined by scanning electron microscope (SEM). For this purpose, small amount of adsorbent particles were taken on stubs with adhesive carbon taps ( $1.15$  cm  $\times$   $0.9$  cm), and SEM images of the adsorbent were taken using 30 KV SEM (JSM5910, JEOL, Tokyo, Japan). UV/Vis spectrophotometer (sp-3000 plus, optima Tokyo, Japan) and pH meter (WTW pH 422) were used in this study.

Table 1  
The maximum acceptable concentrations and aesthetic objectives for four chlorophenols in drinking water

Chlorophenols	Maximum acceptable concentrations		Aesthetic objectives	
	mg/L	$\mu\text{g/L}$	mg/L	$\mu\text{g/L}$
2,4-Dichlorophenol	0.9	900	$\leq 0.0003$	$\leq 0.3$
2,4,6-Trichlorophenol	0.005	5	$\leq 0.002$	$\leq 2$
2,3,4,6-Tetrachlorophenol	0.1	100	$\leq 0.001$	$\leq 1$
Pentachlorophenol	0.06	60	$\leq 0.030$	$\leq 30$

### 2.3. Conditions of HPLC

A Perkin Elmer HPLC series 200, with UV/Vis detector was operated at 25°C using a flow rate of 1 mL/min and wavelength 254 nm for the simultaneous analysis of 2,4-DCP and 2,4,6-TCP with acetonitrile:methanol:water (40:35:25) as mobile phase. The volume of sample injection used was 20  $\mu$ L. A representative chromatogram for the separation of the two phenols is shown in Fig. 2. The analytical parameters of the HPLC method are given in Table 2.

### 2.4. Synthesis of $Fe_3O_4$ magnetic nanoparticles

$Fe_3O_4$  magnetic nanoparticles were prepared by co-precipitation method. Iron(II) sulfate hepta hydrate (4.2 g) and iron(III) chloride (6.3 g) were mixed in a ratio of 1:2 in 400 mL of distilled water. The mixture was heated at 80°C

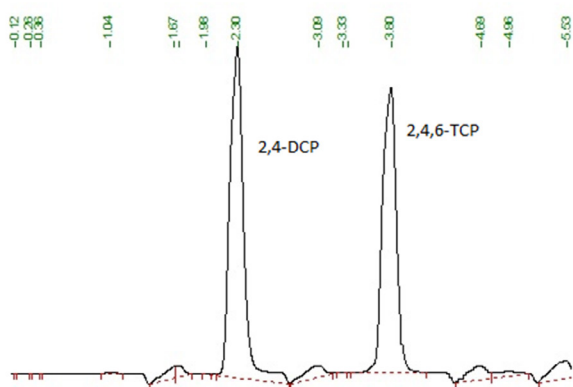


Fig. 2. Representative chromatogram for the simultaneous separation of 2,4-DCP and 2,4,6-TCP.

Table 2

Analytical parameters of the HPLC method

Analytes	Linearity range ( $\mu$ g/mL)	Calibration equation	Correlation coefficient	RSD %	Limit of detection ( $\mu$ g/mL)	Limit of quantification ( $\mu$ g/mL)
2,4-DCP	0.5–20	$y = 0.0122x - 0.0036$	0.9986	0.56	0.03	0.09
2,4,6-TCP	0.5–20	$y = 0.0101 + 0.0039$	0.9983	0.27	0.02	0.05

for 1 h on water bath. To this solution (wine red in color) was added 40 mL of ammonia, which resulted in the formation of black precipitate of  $Fe_3O_4$ . It was further heated for 30 min at 80°C on water bath for digestion.  $Fe_3O_4$  nanoparticles were then filtered out, washed with ethanol and dried in furnace at 150°C. The dried precipitates were crushed and grinded using pestle and mortar to obtain uniform particle size and stored in the glass vials at room temperature.

### 2.5. PANI coating over iron magnetic nanoparticles

Iron magnetic nanoparticles (1 g) were added to a 200 mL of distilled water. About 0.6 mL of aniline was added to it. The pH was adjusted to 3 with hydrochloric acid (0.1 N) solution, and then added 50 mL of 1.2% potassium persulphate. The solution was left for 10 h at room temperature for the completion of polymerization reaction. After 10 h, the solution appeared to be green which was filtered,  $Fe_3O_4$ @PANI nanocomposite were washed first with ethanol to remove the organic impurities and then with water to remove inorganic impurities and excess acid. Washing was continued till neutral point was reached (pH = 7). Then,  $Fe_3O_4$ @PANI nanocomposite was dried, stored, and used for adsorption study. The schematic representation for the preparation of  $Fe_3O_4$ @PANI nanocomposite is shown in Fig. 3.

## 3. Results and discussion

### 3.1. Surface area determination for iron magnetic nanoparticles and $Fe_3O_4$ @PANI nanocomposite

Accurately weighted iron magnetic nanoparticles of 0.5 g was taken in 100 mL of titration flask, to this was added 10 mL (0.1 N) of standardized iodine solution and then stirred for 30 min on orbital shaker. After stirring it was diluted to final volume of 50 mL with distilled water and kept for 0.5 h.

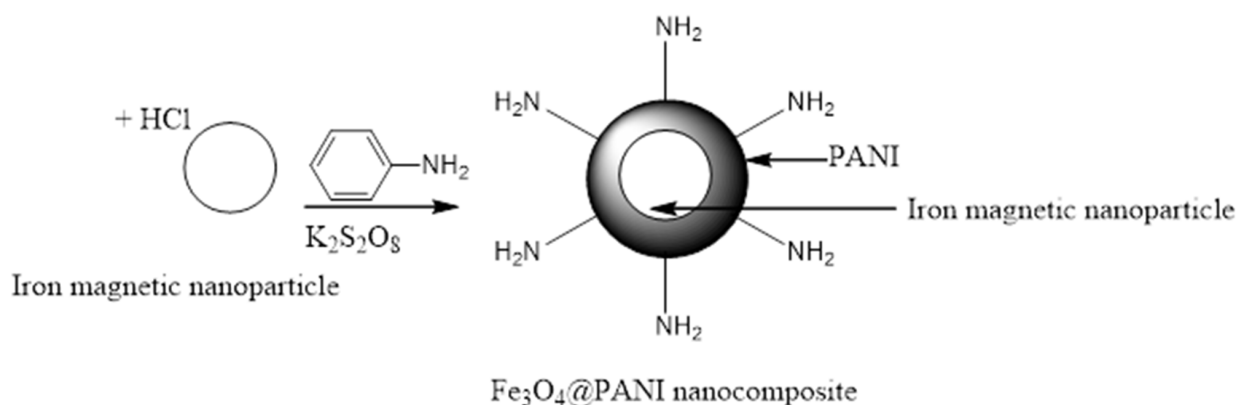


Fig. 3. Schematic representation for the preparation of  $Fe_3O_4$ @PANI nanocomposite.

After equilibration, solutions were filtered with Whatman filter paper 42, and unadsorbed iodine was determined by taking 10 mL of filtrate and titrated with standardized sodium thiosulphate solution, using starch as an indicator. The surface area of uncoated iron magnetic nanoparticles was found to be  $186.086 \text{ m}^2\text{g}^{-1}$ , and  $\text{Fe}_3\text{O}_4@ \text{PANI}$  nanocomposite was found to be  $168.0156 \text{ m}^2\text{g}^{-1}$ .

### 3.2. XRD analysis

The XRD patterns of both iron magnetic nanoparticles and  $\text{Fe}_3\text{O}_4@ \text{PANI}$  nanocomposite were taken. The XRD for iron magnetic nanoparticles and  $\text{Fe}_3\text{O}_4@ \text{PANI}$  nanocomposite is shown in Fig. 4 and its pattern according to ICDD number 11053, 130088, 130091, 130458, 130534, and 160653 shows peak from  $5^\circ$  to  $80^\circ$ . Height, area of the peak, and their respective thickness was calculated by the Scherer's equation, it was observed that  $2\Theta$  values for major reflections ranges from  $7.5^\circ$  to  $77^\circ$ . The thicknesses of the crystal lattice calculated by Scherer's equation demonstrated that crystal thickness ranges from 1.287 to 654.60 nm. By applying Bragg's law, particle to particle distance ( $d$ ) was found to be in the range of 0.247 to 2.355 nm.

### 3.3. EDX analysis

The EDX analysis of both iron magnetic nanoparticles and  $\text{Fe}_3\text{O}_4@ \text{PANI}$  nanocomposite is presented in Fig. 5, where it can be seen that the carbon content of  $\text{Fe}_3\text{O}_4$  increased from 2.36% to 28.24% after being coated with PANI.

### 3.4. Surface morphology

The size and morphology of the  $\text{Fe}_3\text{O}_4@ \text{PANI}$  nanocomposite were determined by SEM at 10,000 magnification. As shown in Fig. 6, the  $\text{Fe}_3\text{O}_4@ \text{PANI}$  nanocomposite has a nearly spherical shape with a smooth and uniform surface morphology. The particles seemed agglomerated and having size of about  $1 \mu\text{m}$ .

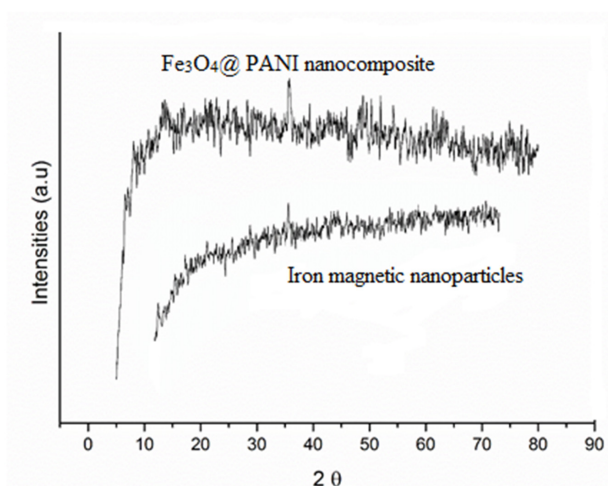


Fig. 4. XRD spectra of iron magnetic nanoparticles and  $\text{Fe}_3\text{O}_4@ \text{PANI}$  nanocomposite.

### 3.5. FTIR analysis

Fourier-transform infrared spectroscopy (FTIR) spectral analysis shows the surface chemistry of the iron magnetic nanoparticles and  $\text{Fe}_3\text{O}_4@ \text{PANI}$  nanocomposite (Fig. 7). The FTIR spectra shows the presence of  $\text{Fe}_3\text{O}_4$  through the presence of two strong adsorption bands at  $403$  and  $667 \text{ cm}^{-1}$ , which correspond to Fe–O bonds depicting stretching frequencies of tetrahedral and octahedral sites, respectively. The bands at  $3,030.16$  and  $3,167.11 \text{ cm}^{-1}$  have been assigned to the stretching and bending vibrations of H–O–H bond, respectively, showing the physical adsorption of water molecules on the surface of the nanoparticles. The strong IR peaks at  $555.499 \text{ nm}$  correspond to the stretching vibration mode of Fe–O bands in iron magnetic nanoparticles. In the spectra, there are some additional peaks, which belong to PANI coating of iron magnetic nanoparticles. The peak appeared at  $1,465.9 \text{ nm}$  is related to C–N absorption band. The peak at  $1,604.77 \text{ nm}$  is attributed to the bending vibration of aromatic C–C bonds of PANI. The peaks centered at  $2,322.29$  and  $1,049.86 \text{ nm}$  are due to the stretching and bending vibrations of C–H bonds of PANI, respectively. A broad absorption band resulted from the N–H bonds can be observed at  $3,433.763 \text{ nm}$ . The results revealed the presence of PANI coating on the iron magnetic nanoparticles.

### 3.6. Point of zero charge determination for iron magnetic nanoparticles and $\text{Fe}_3\text{O}_4@ \text{PANI}$ nanocomposite

pH 2–10 was adjusted (by using hydrochloric acid [0.05 M] and sodium hydroxide [0.05 M] solution) in separate titration flasks containing 20 mL solution of sodium chloride (0.1 M). Then 0.1 g of iron magnetic nanoparticles was added to each flask. For thorough mixing, solutions were placed on orbital shaker for 1 h at 200 rpm, and its pH was measured. Then these

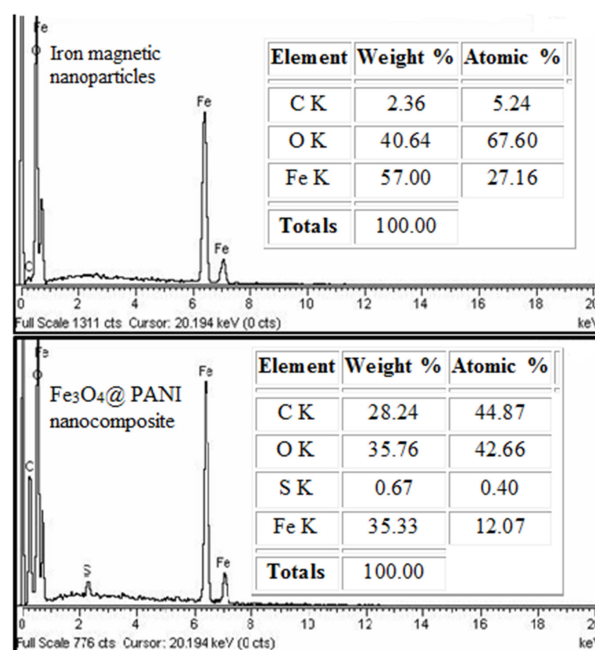


Fig. 5. Elemental composition of iron magnetic nanoparticles and  $\text{Fe}_3\text{O}_4@ \text{PANI}$  nanocomposite.

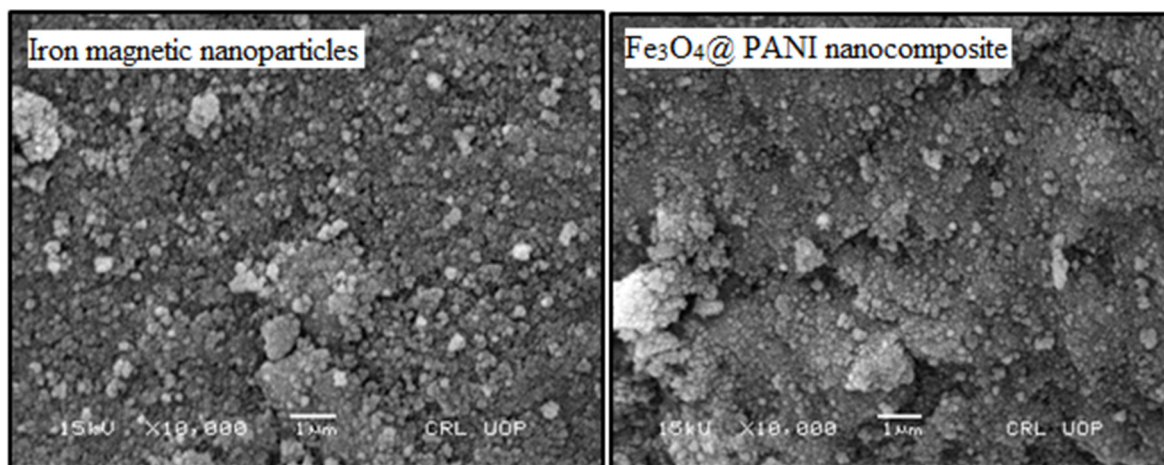


Fig. 6. SEM of iron magnetic nanoparticles and  $\text{Fe}_3\text{O}_4$ @PANI nanocomposite.

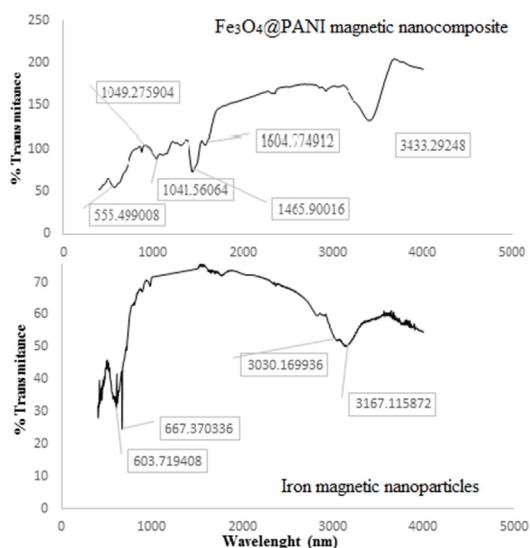


Fig. 7. FTIR spectra of iron magnetic nanoparticles and  $\text{Fe}_3\text{O}_4$ @PANI nanocomposite.

solutions were left for 24 h without shaking and its pH was measured again, initial pH was plotted against  $\Delta\text{pH}$  to determine the point of zero charge. The same procedure was used for determining the point of zero charge for  $\text{Fe}_3\text{O}_4$ @PANI nanocomposite. The results for iron magnetic nanoparticles and  $\text{Fe}_3\text{O}_4$ @PANI nanocomposite are shown in Fig. 8. The point of zero charge for iron magnetic nanoparticles and  $\text{Fe}_3\text{O}_4$ @PANI nanocomposite was found to be 4.9 and 3.5, respectively.

### 3.7. Effect of pH on adsorption of 2,4-DCP and 2,4,6-TCP on iron magnetic nanoparticles and $\text{Fe}_3\text{O}_4$ @PANI nanocomposite

Britton Robinson buffer solutions of pH in the range of 2–10 were prepared and used for this purpose.  $\text{Fe}_3\text{O}_4$ @PANI nanocomposite of 0.05 g were weighed in a series of beakers, 5 mL of 100  $\mu\text{g}/\text{mL}$  solution of 2,4-DCP was added to each beaker, followed by the addition of 2 mL of Britton Robinson buffer in the range of 2–10 pH, respectively, and diluted up to

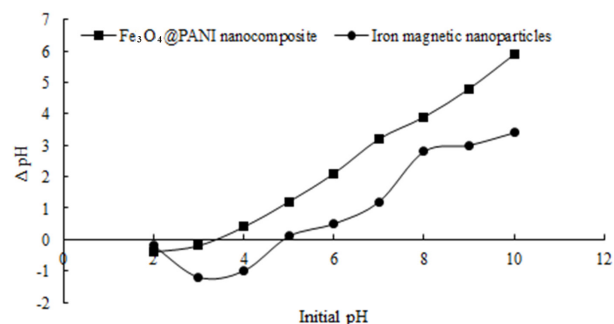


Fig. 8. Point of zero charge for iron magnetic nanoparticles and  $\text{Fe}_3\text{O}_4$ @PANI nanocomposite.

25 mL with distilled water. All the solutions were equilibrated for 1 h. After filtration, the filtrate was obtained which contained the unadsorbed 2,4-DCP. The filtrate was injected to HPLC and the absorbance was checked. As can be seen from the graph (Fig. 9(b)), there is no effect of pH on adsorption. The same procedure was repeated for adsorption of 2,4,6-TCP on  $\text{Fe}_3\text{O}_4$ @PANI nanocomposite, percentage adsorption was almost the same (~94%) at all pH. The adsorbent ( $\text{Fe}_3\text{O}_4$ @PANI nanocomposite) is negatively charged at pH greater than its point of zero charge (3.5). Therefore, it is positively charged at  $\text{pH} < 3.5$  and negatively charged at  $\text{pH} > 3.5$ . This indicates that adsorption of 2,4-DCP and 2,4,6-TCP on  $\text{Fe}_3\text{O}_4$ @PANI composite may be due to hydrogen bonding of  $-\text{OH}$  group from phenols and  $-\text{N}$  of PANI. It may be also be due to van der Waal's forces or it may be due to a donor-acceptor complex formation, the lone pair of electrons is donated by nitrogen of  $\text{Fe}_3\text{O}_4$ @PANI composite, whereas the aromatic ring of phenol act as an acceptor. Therefore pH 6 was selected for simultaneous adsorption of these chlorophenols.

### 3.8. Effect of contact time on adsorption of 2,4-DCP and 2,4,6-TCP on $\text{Fe}_3\text{O}_4$ @PANI nanocomposite

Adsorbent (0.1 g) was taken in series of beakers, 10 mL of 100  $\mu\text{g}/\text{mL}$  2,4-DCP solution was added to each beaker. Britton Robinson buffer of pH 6 (2 mL) was added to it, then

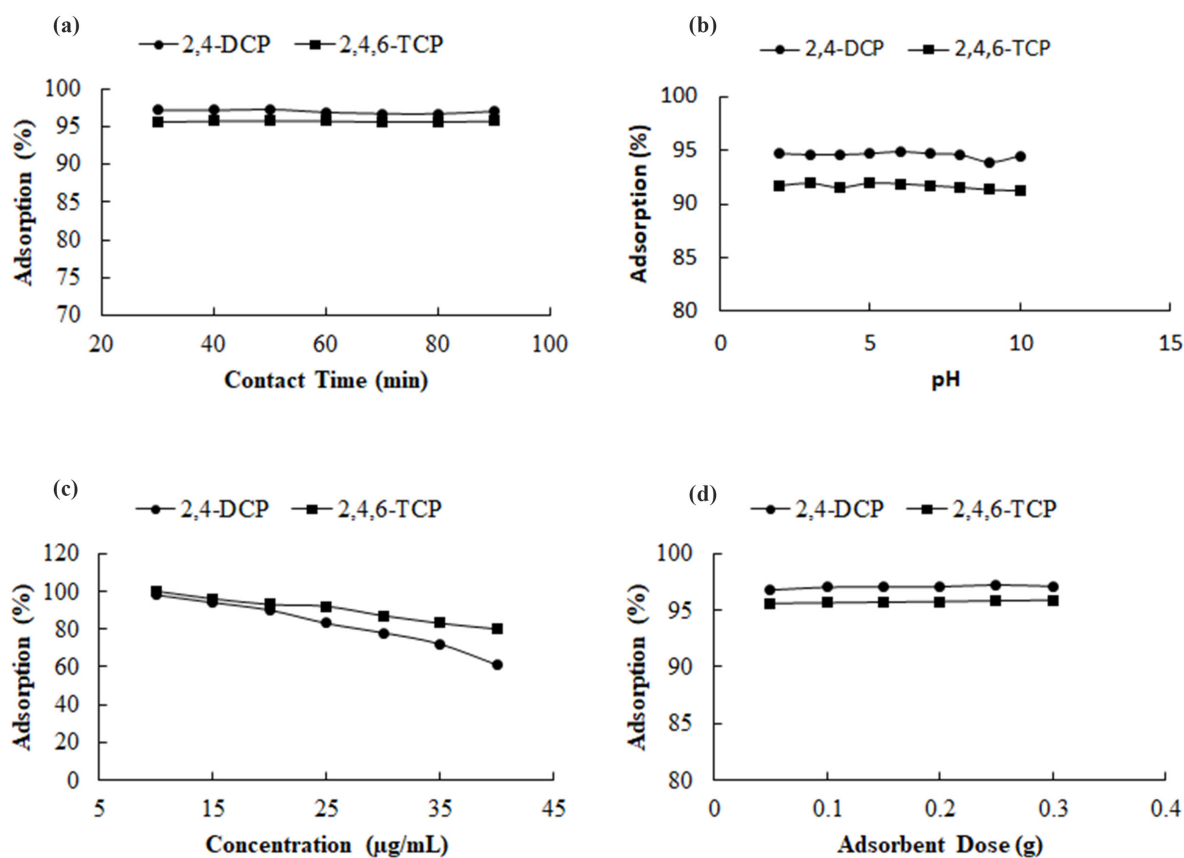


Fig. 9. (a) Effect of contact time on adsorption of 2,4-DCP and 2,4,6-TCP on Fe<sub>3</sub>O<sub>4</sub>@PANI nanocomposite, (b) effect of pH on adsorption of 2,4-DCP and 2,4,6-TCP on Fe<sub>3</sub>O<sub>4</sub>@PANI nanocomposite, (c) effect of the concentration of 2,4-DCP and 2,4,6-TCP on adsorption of Fe<sub>3</sub>O<sub>4</sub>@PANI nanocomposite, and (d) effect of adsorbent dose as a function of adsorption of 2,4-DCP and 2,4,6-TCP.

solutions were diluted up to 25 mL with distilled water. The solutions were placed on orbital shaker at 120 rpm to equilibrate for 30–90 min at room temperature. With increase in contact time, there is no increase in adsorption capacity. The same procedure was repeated for adsorption of 2,4,6-TCP on Fe<sub>3</sub>O<sub>4</sub>@PANI nanocomposite. The result is shown in Fig. 9(a). As can be seen from the result that contact time has no effect on adsorption of 2,4,6-TCP on Fe<sub>3</sub>O<sub>4</sub>@PANI. Therefore an equilibration time of 30 min was used for simultaneous adsorption of these chlorophenols.

### 3.9. Effect of adsorbent dose (Fe<sub>3</sub>O<sub>4</sub>@PANI nanocomposite) for adsorption of 2,4-DCP and 2,4,6-TCP

Weights of adsorbent in the range of 0.05–0.3 g were taken in separate beakers. 10 mL from 100 µg/mL of 2,4-DCP and 2 mL of buffer of pH 6 was added to each beaker and diluted up to 25 mL with distilled water. All the solutions were agitated for 30 min and the filtered and the unadsorbed 2,4-DCP was monitored on HPLC.

The same procedure was repeated for adsorption of 2,4,6-TCP on Fe<sub>3</sub>O<sub>4</sub>@PANI nanocomposite. The results (Fig. 9(d)) showing that adsorbent dose has no effect on percentage adsorption of 2,4-DCP and 2,4,6-TCP on Fe<sub>3</sub>O<sub>4</sub>@PANI nanocomposite.

### 3.10. Adsorption on Fe<sub>3</sub>O<sub>4</sub>@PANI nanocomposite as a function of adsorbate (2,4-DCP and 2,4,6-TCP) concentration

Fe<sub>3</sub>O<sub>4</sub>@PANI nanocomposite (0.05 g) was taken in a series of beakers. 2,4-DCP solutions in the range of 10–40 ppm were prepared from 100 ppm solution and were added to the beakers followed by the addition of 2 mL of buffer of pH 6 to each beaker. The solutions were diluted up to 25 mL with distilled water and equilibrated for 30 min at room temperature. The same procedure was repeated for adsorption of 2,4,6-TCP on Fe<sub>3</sub>O<sub>4</sub>@PANI nanocomposite. The results are shown diagrammatically in Fig. 9(c). As can be seen from the results sorption capacity of Fe<sub>3</sub>O<sub>4</sub>@PANI nanocomposite decreases with increase in the concentration of 2,4-DCP and 2,4,6-TCP, which shows that at the surface of adsorbent, active sites are occupied by the chlorophenols molecules. At a concentration up to 25 µg/mL for 2,4-DCP and 2,4,6-TCP, the sorption remains 100%, further increase in the concentration resulted in slight decrease of sorption by the nanocomposites.

### 3.11. Effect of temperature for adsorption of 2,4-DCP and 2,4,6-TCP on Fe<sub>3</sub>O<sub>4</sub>@PANI nanocomposite

Fe<sub>3</sub>O<sub>4</sub>@PANI nanocomposite was weighed (0.05 g) in a series of beakers. 5 mL of 2,4-DCP solution from 100 ppm was added to each beaker, and 2 mL of buffer of pH 6 was added

to each beaker and diluted up to 25 mL with distilled water. Water bath was heated at constant temperature in the range of 30°C–60°C. After heating for 30 min, the solutions were filtered. Adsorption was maximum at room temperature and then it decreases with increase in temperature which shows that adsorption of 2,4-DCP on  $\text{Fe}_3\text{O}_4$ @PANI nanocomposite is an exothermic process. Same results were obtained for 2,4,6-TCP. This suggests that energy is taken up by the nearby molecules adsorbed on active site, due to this thermal agitation these molecules get desorbed and adsorption decreased. In the adsorption process, a point is reached at which both forces balance each other and a dynamic equilibrium is established.

### 3.12. Adsorption kinetic models

The kinetic adsorption data were processed to understand the dynamics of the adsorption process of 2,4-DCP and 2,4,6-TCP in terms of the order of the rate constant. Three kinetic models were used (Fig. 10).

#### 3.13. Pseudo-first-order kinetic model

Kinetic data were treated with pseudo-first-order kinetic model and the linear form is as follows:

$\log(q_e - q_t) = \log q_e - k_1 t / 2.303$ ,  $q_e$  or  $q_t = (C_i - C_e) / m \times v$ , where  $q_e$  = amount of phenols adsorbed at equilibrium (30 min),  $q_t$  = amount of phenols adsorbed at any time,  $k_1$  = pseudo-first-order rate constant for adsorption,  $C_i$  = initial

concentration of phenols,  $C_e$  = final concentration of phenols,  $m$  = weight of sorbent used in time studies, and  $v$  = final volume of the filtrate, optimum time = 50 min. Values of the rate constant,  $k_1$ , equilibrium sorption capacity,  $q_e$ , and the rate correlation coefficient,  $R^2$ , were calculated from the plot of  $\log(q_e - q_t)$  vs.  $t$ . The value of sorption rate constant ( $k_1$ ) for 2,4-DCP sorption on  $\text{Fe}_3\text{O}_4$ @PANI nanocomposite was  $-0.0078302 \text{ min}^{-1}$  and for 2,4,6-TCP was  $0.0364 \text{ min}^{-1}$ . The calculated  $q_e$  was not in agreement with the experimental  $q_e$  and, therefore, the sorption of 2,4-DCP and 2,4,6-TCP on  $\text{Fe}_3\text{O}_4$ @PANI nanocomposite sorbent is not ideal pseudo-first-order reactions, also confirmed by the  $R^2$  values of 0.0134 and 0.1266 for sorption of 2,4-DCP and 2,4,6-TCP, respectively.

#### 3.14. Pseudo-second-order kinetic model

Kinetic data were further treated with the pseudo-second-order kinetic model. The linear form is given as  $t/q_t = 1/k_2 q_e^2 + t/q_e$  where  $q_e$  = amount of phenols adsorbed at equilibrium,  $q_t$  = amount of phenols adsorbed at any time, and  $k_2$  = pseudo-second-order reaction rate constant for sorption. The linear plot of  $t/q_t$  against  $t$  showed a good agreement of experimental data with the pseudo-second-order kinetic model for sorption of phenols. The second-order rate constant,  $k_2$ , and the equilibrium sorption capacity,  $q_e$ , were calculated from the intercept and slope of the plots of  $t/q_t$  against  $t$ . The calculated  $q_e$  (9.7287 and 9.5602  $\text{mg g}^{-1}$ ) value agrees very well with the experimental data for 2,4-DCP

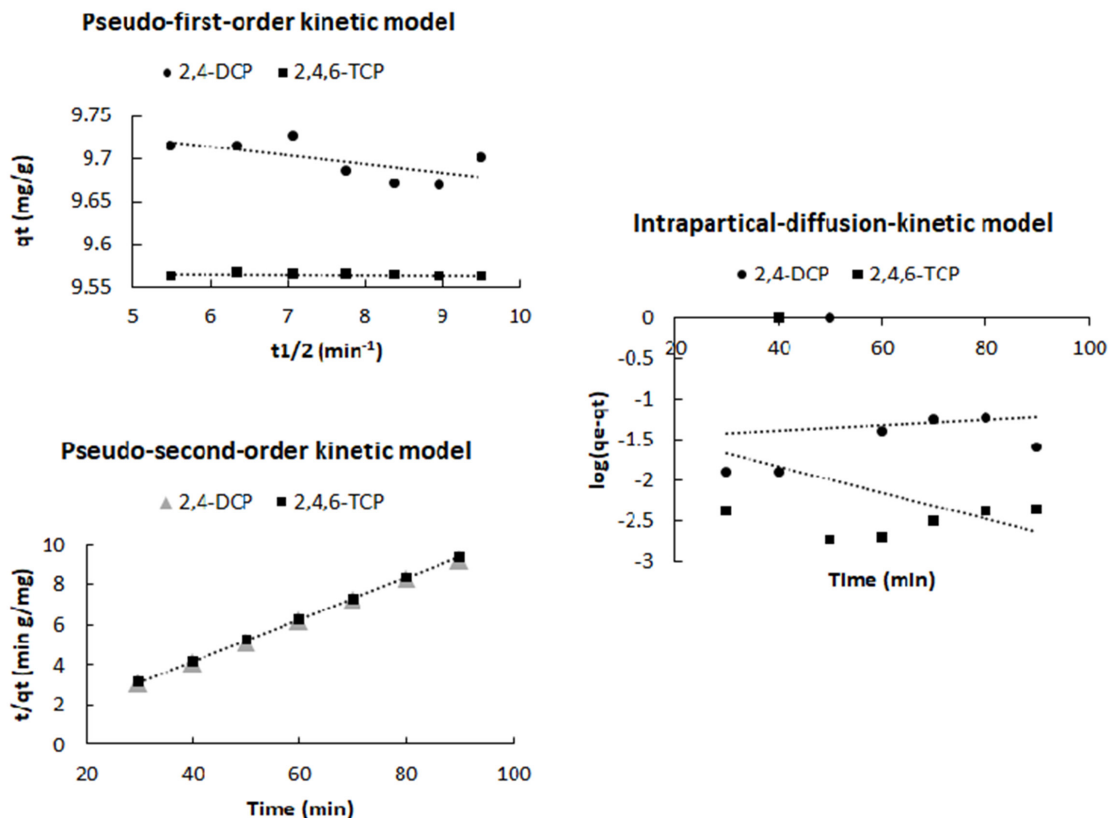


Fig. 10. Pseudo-first-order kinetic model, pseudo-second-order kinetic model, and intraparticle diffusion kinetic model for the adsorption of 2,4-DCP and 2,4,6-TCP on  $\text{Fe}_3\text{O}_4$ @PANI nanocomposite.

and 2,4,6-TCP. The correlation coefficient ( $R^2$ ) for sorption of phenols on  $Fe_3O_4@PANI$  nanocomposite is higher for pseudo-second-kinetic ( $R^2 = 1.00$ ). All of these facts indicate that the sorption of phenols on  $Fe_3O_4@PANI$  nanocomposites sorbent obeys second-order sorption kinetic reactions.

3.15. Intraparticle diffusion kinetic model

Intraparticle diffusion resistance affecting sorption can be explored by using the intraparticle diffusion model,  $q_t = K_{int} t^{1/2} + C$ , where  $C$  is the intercept and related to the thickness of the boundary layer, that is, the larger the value of  $C$ , the greater is the boundary layer effect.  $K_{int}$  is the intraparticle diffusion rate constant ( $mg\ g^{-1}\ min^{-1}$ ), and its value is calculated directly from the slope. The figure shows that the plot of  $q_t$  vs.  $t^{1/2}$  is not passing through the origin and the value for intraparticle diffusion rate constant ( $K_{int} = -mg\ g^{-1}\ min^{-1}$ ) which indicates that the intraparticle diffusion is not the controlling step during sorption of phenols on  $Fe_3O_4@PANI$  nanocomposite.

3.16. Thermodynamic study

To estimate the effect of temperature on the sorption of 2,4-DCP on  $Fe_3O_4@PANI$  nanocomposite, the free energy change ( $\Delta G^\circ$ ), enthalpy change ( $\Delta H^\circ$ ), and entropy change ( $\Delta S^\circ$ ) were determined using the equation,  $\ln K_D = -\Delta H^\circ/RT + \Delta S^\circ/R$ . Thermodynamic parameters were calculated for determination of sorption process, to see if the sorption occurred spontaneously or not. The values of  $K_D$  and  $\Delta G^\circ$  were calculated from sorption of phenols on  $Fe_3O_4@PANI$  nanocomposite from the slope and intercept of van't Hoff's plot. The results for  $\ln$  of  $K_D$  values are given in Table 4. The negative value of  $\Delta H^\circ$  indicates the exothermic sorption process. The negative value of  $\Delta S^\circ$  shows decrease in randomness at solid/solution interface during sorption of 2,4-DCP and 2,4,6-TCP on  $Fe_3O_4@PANI$  nanocomposite. The negative  $\Delta G^\circ$  value of phenols at different temperatures is due to the spontaneous sorption of process of these chlorophenols on  $Fe_3O_4@PANI$  nanocomposite, and the negative value of  $\Delta G^\circ$  decreased with an increase in temperature, indicating that the spontaneous nature of 2,4-DCP and 2,4,6-TCP adsorption is inversely proportional to the temperature.

Table 3  
Isotherms parameters for the adsorption of 2,4-DCP and 2,4,6-TCP on  $Fe_3O_4@PANI$  nanocomposite

Parameter	Values	
	2,4-DCP	2,4,6-TCP
Freundlich sorption isotherm		
$K_f$	0.00007967	3.389
$n$	0.2206	3.134
$R^2$	0.9681	0.9124
Langmuir sorption isotherm		
$K_L$ ( $L\ g^{-1}$ )	0.06566	1.379
$a^L$ ( $L\ mg^{-1}$ )	-0.06944	0.0979
$Q^\circ$ ( $mg\ g^{-1}$ )	-0.9455	14.085
$R^2$	0.8737	0.9694

3.17. Sorption equilibrium study

The analysis of sorption process requires equilibrium study to better understand the sorption process. Equilibrium isotherm equations are used to describe the experimental sorption data. Sorption isotherms also provide fundamental physiochemical data for evaluating the applicability of sorption process. Analysis of the equilibrium data is important to develop an equation which accurately represents the results which could be used for design purpose. An adsorption isotherm is characterized by certain constants, the value of which expresses the surface properties, and affinity of the sorbent can also be used to find the sorptive capacity of sorbent. The two common equilibrium models, that is, Freundlich equilibrium isotherm and Langmuir equilibrium isotherm models have been applied.

3.18. Freundlich sorption isotherm

Freundlich isotherm model can be used for non-ideal sorption and describes sorption for heterogeneous surfaces. It is expressed as follows:  $\log q_e = \log K_f + 1/n \log C_e$ . Freundlich sorption isotherm was drawn for sorbent  $Fe_3O_4@PANI$  nanocomposite by plotting  $\log q_e$  vs.  $\log C_e$  as shown in Fig. 11. Where,  $K_f$  = maximum sorption capacity,  $1/n$  = adsorption intensity,  $n$  = deviation from linearity, and  $C_e$  = equilibrium concentration. Freundlich sorption isotherm was drawn for  $Fe_3O_4@PANI$  nanocomposite by plotting  $\log q_e$  vs.  $\log C_e$  (Fig. 11). The Freundlich model in this case does not provide information of maximum sorption capacity.

3.19. Langmuir sorption isotherm

Langmuir sorption isotherm is one of the widely used sorption isotherm for the sorption of a solute from liquid solution. A basic assumption of the Langmuir theory is that sorption takes place at specific homogeneous sites within the sorbent. It is expressed in its linear form as follows:  $C_e/q_e = 1/K_L + a_L C_e/q_e$ , where  $K_L$  and  $a_L$  are the Langmuir sorption isotherm constants and are related to the maximum capacity ( $L/g$ ) and bonding strength ( $Lg/mg$ ), respectively.  $Q^\circ$  is the maximum sorption capacity and is numerically equal to  $K_L a_L$ . The values of  $K_L$ ,  $a_L$ , and  $Q^\circ$  were calculated from linear plot of  $C_e/q_e$  vs.  $C_e$ . The different values of  $C_e$  and  $C_e/q_e$  are shown in Fig. 11, while the plot of  $C_e$  vs.  $C_e/q_e$  is shown in figure. Table 3 summarizes the results of the two isotherms for sorption of

Table 4  
Thermodynamic parameters for adsorption of 2,4-DCP and 2,4,6-TCP on  $Fe_3O_4@PANI$  nanocomposite

Adsorbate type	Temperature (K)	$\Delta H^\circ$ (KJ/mol)	$\Delta S^\circ$ (KJ/mol)	$\Delta G^\circ$ (KJ/mol)
2,4-DCP	313.15	-6.9814	-23.768	-6,783.86
	323.15			-7,000.76
	333.15			-7,217.66
2,4,6-TCP	343.15	-48.4848	-0.15919	-7,434.56
	313.15			-0.65939
	323.15			-0.849271
	333.15			-1.829031
	343.15			-4.376381

phenols on  $\text{Fe}_3\text{O}_4$ @PANI. The maximum sorption capacity was found with Langmuir isotherm for these phenols.

### 3.20. Desorption study

Desorption studies help to elucidate the mechanism and recovery of the adsorbate and adsorbent. Depending on the nature of the adsorbent/adsorbent-to-surface bond, there are a multitude of mechanisms for desorption. The surface bond of adsorbent can be cleaved thermally, through chemical reactions or by radiation, all of which may result in desorption of the species.

### 3.21. Desorbing solvent

For desorption, 0.2 N sodium hydroxide, pure ethanol, methanol, mixture of ethanol and sodium hydroxide (50:50), mixture of methanol and sodium hydroxide (50:50) were used as desorbing solvents. The process was carried out in two steps: adsorption step and desorption step. In desorption step, the already loaded  $\text{Fe}_3\text{O}_4$ @PANI nanocomposite were agitated with the desorbing solvents. The percentage desorption for each desorption solvent was calculated from equation; data are given in Table 5,  $D = \frac{\text{desorbed } \mu\text{g}}{\text{adsorbed } \mu\text{g}} \times 100$ . The results indicated that mixture of ethanol with sodium hydroxide is an effective desorption solvent for the recovery of phenols from  $\text{Fe}_3\text{O}_4$ @PANI nanocomposite. It is evident from the adsorption equilibrium studies that physisorption (multilayer formation) is a dominant phenomenon whereas chemisorption (monolayer formation) may also occur simultaneously side by side, which is irreversible as compared with physisorption. Therefore, only physically adsorbed 2,4-DCP is desorbed while chemically adsorbed is left behind as such. With the mixture of ethanol + sodium hydroxide maximum amount of adsorbed phenols are removed. As these two chlorophenols are organic polar compound and their solubility is high in methanol and ethanol,

whereas sodium hydroxide convert acid into salt (2,4-dichloro-sodium phenolate ion), thus increasing its solubility by breaking H-bond (physical adsorption). Therefore, ethanol + sodium hydroxide mixture was used for recovery of sorbent.

### 3.22. Application

Matrix effects can influence the ability of an analytical method to qualitatively identify and quantitatively measure target compounds in environmental and other samples by indirectly affecting the intensity and resolution of observed signals. The most common approach accounting for matrix effects is to plot a calibration curve using standard samples with known analyte concentration and which try to approximate the matrix of the sample as much as possible by standard addition method.

### 3.23. Salt effect

Wastewater contains different cations, and it is important to study the competitive adsorption of these coexisting cations. For example, K, Na, Ca(II), Mg(II), Cr(III), and Cu(II) can be present in any water sample and may affect adsorption capacity of chlorophenols on  $\text{Fe}_3\text{O}_4$ @PANI. For studying salt effect, two types of salts were studied, monovalent salt and divalent salt, that is, sodium chloride and calcium chloride.

As can be seen from the results given in Table 6, there is no effect of coexisting cations on the adsorption capacity of chlorophenols (500  $\mu\text{g}$ ) when the concentration of sodium chloride and calcium chloride salt solutions was 0.2 M.

Table 5

Effect of various desorption solvent on percentage recovery of 2,4-DCP and 2,4,6-TCP from  $\text{Fe}_3\text{O}_4$ @PANI nanocomposite

S. no.	Desorbing solvent	Recovery (%)	
		2,4-DCP	2,4,6-TCP
1	Ethanol	25.301	30.02
2	NaOH and ethanol (50:50)	45.619	18.75
3	Methanol	25.460	22.26
4	NaOH and methanol (50:50)	4.190	10.27
5	NaOH (0.2 M)	8.634	15.40

Table 6

Adsorption of 2,4-DCP and 2,4,6-TCP on  $\text{Fe}_3\text{O}_4$ @PANI magnetic nanocomposite in the presence of interference ions using tap water

Adsorbate type	Interfering ions	$\mu\text{g}$ added	$\mu\text{g}$ adsorbed	Adsorption (%)
2,4-DCP and 2,4,6-TCP	Control	500	500	100
	NaCl (0.01 M)	500	500	100
	NaCl (0.1 M)	500	500	100
2,4-DCP	NaCl (0.2 M)	500	500	100
	CaCl <sub>2</sub> (0.01 M)	500	500	100
	CaCl <sub>2</sub> (0.1 M)	500	500	100
2,4,6-TCP	CaCl <sub>2</sub> (0.2 M)	500	500	100

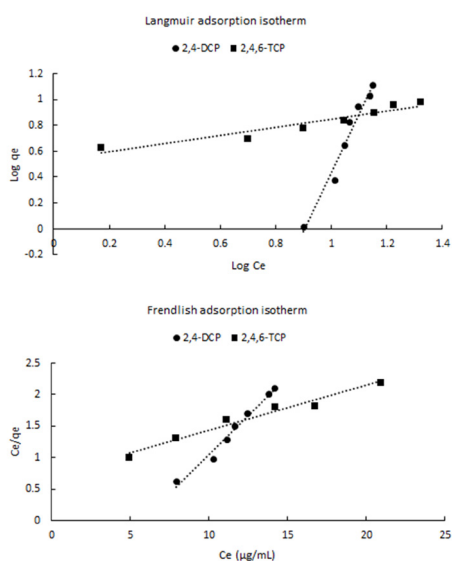


Fig. 11. Freundlich and Langmuir adsorption isotherm models for adsorption 2,4-DCP and 2,4,6-TCP on  $\text{Fe}_3\text{O}_4$ @PANI nanocomposite.

#### 4. Conclusions

This work shows that  $\text{Fe}_3\text{O}_4/\text{PANI}$  is a good choice to be used as adsorbent for removal of 2,4-DCP and 2,4,6-TCP in aqueous medium. The results showed that adsorption of 2,4-DCP and 2,4,6-TCP is pH independent. The equilibrium data for adsorption revealed Freundlich isotherm model. Moreover adsorption of phenols followed pseudo-second-order kinetic model with  $R^2 = 1.0$ . Intraparticle diffusion is not controlling step for the adsorption of 2,4-DCP and 2,4,6-TCP on  $\text{Fe}_3\text{O}_4/\text{PANI}$  nanocomposite. The thermodynamic parameters indicated that the adsorption process of phenols was exothermic and spontaneous but at low temperature with decrease in randomness at the solid/liquid interface. The presence of coexisting metals ions has no effect on the removal efficiency of 2,4-DCP and 2,4,6-TCP from the aqueous solution. The method is highly selective as there are no significant interferences at all from matrix cations even at high concentration up to 0.2 M.  $\text{Fe}_3\text{O}_4/\text{PANI}$  nanocomposite not only showed high adsorption capacity and rapid kinetics but also follows a simple inexpensive adsorbent preparation, which is environment friendly.

#### References

- [1] X.G. Li, A. Li, M.R. Huang, Facile high-yield synthesis of polyaniline nanosticks with intrinsic stability and electrical conductivity, *Chem. Eur. J.*, 14 (2008) 10309–10317.
- [2] M. Saad, H. Tahir, J. Khan, U. Hameed, A. Saud, Synthesis of polyaniline nanoparticles and their application for the removal of crystal violet dye by ultrasonicated adsorption process based on response surface methodology, *Ultrason. Sonochem.*, 34 (2017) 600–608.
- [3] A. Mehdinia, R. Esfandiarnjad, A. Jabbari, Magnetic nanocomposite of self-doped polyaniline-graphene as a novel sorbent for solid-phase extraction, *J. Sep. Sci.*, 38 (2015) 141–147.
- [4] M. Sboui, M.F. Nsib, A. Rayes, M. Swaminathan, A. Houas,  $\text{TiO}_2\text{-PANI/Cork}$  composite: a new floating photocatalyst for the treatment of organic pollutants under sunlight irradiation, *J. Environ. Sci.*, 60 (2017) 3–13.
- [5] V. Sharma, P. Rekha, P. Mohanty, Nanoporous hypercrosslinked polyaniline: an efficient adsorbent for the adsorptive removal of cationic and anionic dyes, *J. Mol. Liq.*, 222 (2016) 1091–1100.
- [6] H. Javadian, Application of kinetic, isotherm and thermodynamic models for the adsorption of  $\text{Co(II)}$  ions on polyaniline/polypyrrole copolymer nanofibers from aqueous solution, *J. Ind. Eng. Chem.*, 20 (2014) 4233–4241.
- [7] B. Qiu, C. Xu, D. Sun, H. Wei, X. Zhang, J. Guo, Q. Wang, D. Rutman, Z. Guo, S. Wei, Polyaniline coating on carbon fiber fabrics for improved hexavalent chromium removal, *RSC Adv.*, 4 (2014) 29855.
- [8] B. Qiu, C. Xu, D. Sun, Q. Wang, H. Gu, X. Zhang, B.L. Weeks, J. Hopper, T.C. Ho, Z. Guo, S. Wei, Polyaniline coating with various substrates for hexavalent chromium removal, *Appl. Surf. Sci.*, 334 (2015) 7–14.
- [9] S. Su, B. Chen, M. He, B. Hu, Z. Xiao, Determination of trace/ultratrace rare earth elements in environmental samples by ICP-MS after magnetic solid phase extraction with  $\text{Fe}_3\text{O}_4/\text{SiO}_2/\text{polyaniline-graphene}$  oxide composite, *Talanta.*, 119 (2014) 458–466.
- [10] L. Ai, J. Jiang, R. Zhang, Uniform polyaniline microspheres: a novel adsorbent for dye removal from aqueous solution, *Synth. Met.*, 160 (2010) 762–767.
- [11] M. M. Ayad, A.A. El-Nasr, Adsorption of cationic dye (methylene blue) from water using polyaniline nanotubes base, *J. Phys. Chem. C*, 114 (2010) 14377–14383.
- [12] M. Ayad, S. Zaghlol, Nanostructured crosslinked polyaniline with high surface area: synthesis, characterization and adsorption for organic dye, *Chem. Eng. J.*, 204–205 (2012) 79–86.
- [13] N. Gopal, M. Asaithambi, P. Sivakumar, V. Sivakumar, Adsorption studies of a direct dye using polyaniline coated activated carbon prepared from *Prosopis juliflora*, *J. Water Process Eng.*, 2 (2014) 87–95.
- [14] D. Mahanta, G. Madras, S. Radhakrishnan, S. Patil, Adsorption of sulfonated dyes by polyaniline emeraldine salt and its kinetics, *J. Phys. Chem. B*, 112 (2008) 10153–10157.
- [15] R. Saravanan, E. Sacari, F. Gracia, M.M. Khan, E. Mosquera, V.K. Gupta, Conducting PANI stimulated ZnO system for visible light photocatalytic degradation of coloured dyes, *J. Mol. Liq.*, 221 (2016) 1029–1033.
- [16] I. Sowa, M. Pizon, R. Swieboda, R. Kocjan, D. Zajdel, Properties of chelating sorbent prepared by modification of silica gel with polyaniline and acid Alizarin Violet N, *Sep. Sci. Technol.*, 47 (2012) 1194–1198.
- [17] Y. Ai, J. Zhang, F. Zhao, B. Zeng, Hydrophobic coating of polyaniline-poly(propylene oxide) copolymer for direct immersion solid phase microextraction of carbamate pesticides, *J. Chromatogr. A*, 1407 (2015) 52–57.
- [18] P. Arnnok, N. Patdhanagul, R. Burakham, Dispersive solid-phase extraction using polyaniline-modified zeolite NaY as a new sorbent for multiresidue analysis of pesticides in food and environmental samples, *Talanta.*, 164 (2017) 651–661.
- [19] Y. Wang, Y. Sun, Y. Gao, B. Xu, Q. Wu, H. Zhang, D. Song, Determination of five pyrethroids in tea drinks by dispersive solid phase extraction with polyaniline-coated magnetic particles, *Talanta.*, 119 (2014) 268–275.
- [20] X. Yang, K. Qiao, Y. Ye, M. Yang, J. Li, H. Gao, S. Zhang, W. Zhou, R. Lu, Facile synthesis of multifunctional attapulgite/ $\text{Fe}_3\text{O}_4$ /polyaniline nanocomposites for magnetic dispersive solid phase extraction of benzoylurea insecticides in environmental water samples, *Anal. Chim. Acta*, 934 (2016) 114–121.
- [21] X. Yang, K. Qiao, F. Liu, X. Wu, M. Yang, J. Li, H. Gao, S. Zhang, W. Zhou, R. Lu, Magnetic mixed hemimicelles dispersive solid-phase extraction based on ionic liquid-coated attapulgite/polyaniline-polypyrrole/ $\text{Fe}_3\text{O}_4$  nanocomposites for determination of acaricides in fruit juice prior to high-performance liquid chromatography-diode array d, *Talanta.*, 166 (2017) 93–100.
- [22] H. Ding, X. Li, J. Wang, X. Zhang, C. Chen, Adsorption of chlorophenols from aqueous solutions by pristine and surface functionalized single-walled carbon nanotubes, *J. Environ. Sci.*, 43 (2016) 187–198.
- [23] L. Zhang, B. Zhang, T. Wu, D. Sun, Y. Li, Adsorption behavior and mechanism of chlorophenols onto organoclays in aqueous solution, *Colloids Surf., A*, 484 (2015) 118–129.
- [24] K. Mutharasaiah, V. Govindareddy, C. Karigar, Biodegradation of 2-chlorophenol by *Bacillus subtilis* isolated from industrial sludge, *Bioscan*, 6 (2011) 305–309.
- [25] J. Huang, Q. Chang, Y. Ding, X. Han, H. Tang, Catalytic oxidative removal of 2,4-dichlorophenol by simultaneous use of horseradish peroxidase and graphene oxide/ $\text{Fe}_3\text{O}_4$  as catalyst, *Chem. Eng. J.*, 254 (2014) 434–442.
- [26] M. Guo, X. Weng, T. Wang, Z. Chen, Biosynthesized iron-based nanoparticles used as a heterogeneous catalyst for the removal of 2,4-dichlorophenol, *Sep. Purif. Technol.*, 175 (2017) 222–228.
- [27] J. Xu, Z. Cao, X. Liu, H. Zhao, X. Xiao, J. Wu, X. Xu, J.L. Zhou, Preparation of functionalized Pd/Fe- $\text{Fe}_3\text{O}_4$ @MWCNTs nanomaterials for aqueous 2,4-dichlorophenol removal: interactions, influence factors, and kinetics, *J. Hazard. Mater.*, 317 (2016) 656–666.
- [28] J. Xu, Z. Cao, X. Liu, H. Zhao, X. Xiao, J. Wu, X. Xu, J.L. Zhou, Preparation of functionalized Pd/Fe- $\text{Fe}_3\text{O}_4$ @MWCNTs nanomaterials for aqueous 2,4-dichlorophenol removal: interactions, influence factors, and kinetics, *J. Hazard. Mater.*, 317 (2016) 656–666.